



# Preferred Growth Direction by PbS Nanoplatelets Preserves Perovskite Infrared Light Harvesting for Stable, Reproducible, and Efficient Solar Cells

Humberto Emmanuel Sánchez-Godoy, Eider Ansisar Erazo, Andrés Fabián Gualdrón-Reyes, Ali Hossain Khan, Said Agouram, Eva Maria Barea, Rubén Arturo Rodríguez, Isaac Zarazúa, Pablo Ortiz, María Teresa Cortés, Vicente Muñoz-Sanjosé, Iwan Moreels, Sofia Masi,\* and Iván Mora-Seró\*

Formamidinium-based perovskite solar cells (PSCs) present the maximum theoretical efficiency of the lead perovskite family. However, formamidinium perovskite exhibits significant degradation in air. The surface chemistry of PbS has been used to improve the formamidinium black phase stability. Here, the use of PbS nanoplatelets with (100) preferential crystal orientation is reported, to potentiate the repercussion on the crystal growth of perovskite grains and to improve the stability of the material and consequently of the solar cells. As a result, a vertical growth of perovskite grains, a stable current density of  $23 \text{ mA cm}^{-2}$ , and a stable incident photon to current efficiency in the infrared region of the spectrum for 4 months is obtained, one of the best stability achievements for planar PSCs. Moreover, a better reproducibility than the control device, by optimizing the PbS concentration in the perovskite matrix, is achieved. These outcomes validate the synergistic use of PbS nanoplatelets to improve formamidinium long-term stability and performance reproducibility, and pave the way for using metastable perovskite active phases preserving their light harvesting capability.

very promising and efficient material.<sup>[1]</sup> Due to its impressive properties such as a high absorption coefficient, long diffusion length and low exciton dissociation energy,<sup>[2]</sup> the perovskite has been exploited in several applications, among them light amplifiers and lasers,<sup>[3–5]</sup> light emitting diodes (LEDs),<sup>[6–8]</sup> and photovoltaic devices.<sup>[9,10]</sup> The halide perovskite structure,  $\text{ABX}_3$ <sup>[11]</sup> allows multiple atom combinations, making it very versatile. In addition, it can be synthesized at a low temperature permitting a relatively easy synthesis by a broad range of methods. The monovalent cation A (formamidinium [FA],<sup>[12]</sup> methylammonium [MA],<sup>[13]</sup> or cesium<sup>[14]</sup>) is located in the cage of  $\text{BX}_6^{4-}$  octahedra, where B is the metal (commonly, lead or tin) and X a halide or combination of them. The most studied hybrid-perovskite materials


are  $\text{MAPbI}_3$  and  $\text{FAPbI}_3$ . Both compounds result in a perovskite structure, despite the difference in the tolerance factor (0.95 and 1.03, respectively, and the same octahedral factor.<sup>[15,16]</sup>  $\text{MAPbI}_3$  is intrinsically phase stable at ambient

## 1. Introduction

The photovoltaic field has undergone rapid progress in the last 10 years, along with the halide perovskite, that emerged as a

H. E. Sánchez-Godoy, E. A. Erazo, Dr. A. F. Gualdrón-Reyes, Prof. E. M. Barea, Dr. S. Masi, Prof. I. Mora-Seró  
Institute of Advanced Materials (INAM)  
Universitat Jaume I (UJI)  
Avenida de Vicent Sos Baynat, s/n, Castellón de la Plana 12071, Spain  
E-mail: masi@uji.es; sero@uji.es

H. E. Sánchez-Godoy, Dr. R. A. Rodríguez, Dr. I. Zarazúa  
Departamento de Ciencias Exactas y Tecnología  
Centro Universitario de los Lagos  
Universidad de Guadalajara  
Lagos de Moreno C.P. 47460, México

 The ORCID identification number(s) for the author(s) of this article can be found under <https://doi.org/10.1002/aenm.202002422>.

© 2020 The Authors. Advanced Energy Materials published by Wiley-VCH GmbH. This is an open access article under the terms of the Creative Commons Attribution-NonCommercial-NoDerivs License, which permits use and distribution in any medium, provided the original work is properly cited, the use is non-commercial and no modifications or adaptations are made.

DOI: 10.1002/aenm.202002422

E. A. Erazo, Dr. P. Ortiz, Dr. M. T. Cortés  
Departamento de Química  
Universidad de los Andes  
Bogotá D.C. 111711, Colombia  
Dr. A. H. Khan, Prof. I. Moreels  
Department of Chemistry  
Ghent University  
Krijgslaan 281-S3, Ghent 9000, Belgium  
Dr. S. Agouram, Prof. V. Muñoz-Sanjosé  
Department of Applied Physics and Electromagnetism  
University of Valencia  
Valencia 46100, Spain  
Dr. S. Agouram, Prof. V. Muñoz-Sanjosé, Prof. I. Mora-Seró  
Materials for Renewable Energy (MAER)  
Unitat Mixta d'Investigació UV-UJI  
Valencia 46010, Spain

conditions but vulnerable to high temperature.<sup>[17]</sup> In contrast, FAPbI<sub>3</sub> perovskite solar cells (PSCs) are potentially more interesting as they present higher thermal stability and a narrower bandgap, of 1.48 eV,<sup>[18]</sup> near the Shockley–Queisser maximum theoretical performance.<sup>[19]</sup> However the  $\alpha$ -phase (black phase) of FAPbI<sub>3</sub> is less stable under ambient conditions than its  $\delta$ -phase (yellow phase),<sup>[20]</sup> making the study and development of these PSCs highly demanding due to the FAPbI<sub>3</sub> black phase instability.

Despite the desired lower bandgap and the extended absorption onset, FAPbI<sub>3</sub> has a weaker light absorption than MAPbI<sub>3</sub> at wavelengths longer than 700 nm.<sup>[21]</sup> Thus, in order to generate the same current, the layer needs to be thicker. To compensate the weak absorption and the low stability of perovskite, binary mixtures, like MAPbI<sub>3</sub>-FAPbI<sub>3</sub> and CsPbI<sub>3</sub>-FAPbI<sub>3</sub>, respectively, have been exploited.<sup>[22]</sup> The combination of differently sized cations is at the same time a strategy to tune the tolerance factor, to improve the stability of the cubic phase, and to reduce the nonradiative recombination. However, the higher bandgap (1.63 eV for the most representative Cs<sub>0.05</sub>MA<sub>0.16</sub>FA<sub>0.79</sub>Pb(I<sub>0.83</sub>Br<sub>0.17</sub>)<sub>3</sub>) compared to the bare FAPbI<sub>3</sub> (1.48 eV), limits performance, and segregation problems are currently present, inducing some limitations of this method, so usually the amount of the secondary perovskite has to be as low as possible. For instance, when the amount of Cs<sup>+</sup> is higher than 15%,<sup>[23]</sup> CsPbI<sub>3</sub> separates on the top of the FA<sub>1-x</sub>Cs<sub>x</sub>PbI<sub>3</sub> layer, preventing a good contact between perovskite and hole transporting layer, resulting also in a low reproducibility.

A different approach takes advantage from external additives, which minimize the migration of defects, assist the perovskite growth and crystallization process,<sup>[24–26]</sup> leading to an ideal morphology of the perovskite grains,<sup>[27,28]</sup> and reduce the crystal lattice parameter in mixed cation/halide perovskites.<sup>[29]</sup> Among them, inorganic external additives were recently exploited. Chloride incorporated as MACl<sup>[30]</sup> or as methylendiammonium dichloride (MDACL<sub>2</sub>)<sup>[31]</sup> or PbS QDs confer outstanding stability to the FA-based perovskite, without affecting its bandgap.<sup>[32]</sup> Beyond that, inorganic PbS quantum dots (QDs) with similar lattice parameter are incorporated into the perovskite matrix for a bulk-epitaxial growth of the perovskite. The key role of PbS QDs lies at the atomic level, either to promote perovskite crystallization<sup>[33–35]</sup> or to improve the stability, according to a chemi-structural mechanism,<sup>[32]</sup> with the additional benefit of preserving the bandgap of FAPbI<sub>3</sub>. In particular, the structural matching between the FAPbI<sub>3</sub>  $\alpha$ -phase and the (100) PbS facets<sup>[36]</sup> results in a stabilization of the  $\alpha$ -phase with respect to the  $\delta$ -phase.<sup>[32]</sup> To take advantage of the FAPbI<sub>3</sub> black phase stabilization promoted by (100) PbS facets,<sup>[32]</sup> in this work, we have analyzed the use of these nanoplatelets (NPLs) with controlled lateral size and (100) crystal orientation of the basal facets,<sup>[37]</sup> compatible with the stabilization of the  $\alpha$ -phase. The PbS itself is a promising material with weakly bound excitons and tunable optical properties<sup>[38]</sup> in the near infrared spectral region.<sup>[39]</sup> The tunable bandgap (from 0.5 to 1.5 eV) allows for a broad spectral coverage when combined with the perovskite. However PbS with a bandgap lower than 1 eV could limit the solar power generation.<sup>[40]</sup> PbS NPLs, with a bandgap close to the one of the perovskites could regulate this drawback. Moreover, the 2D shape exposes the terminal atom in a preferential direction and could enable a reduction of optical defects in the perovskite host.<sup>[37]</sup> In addition, it has been demonstrated that 2D materials such as MXene,<sup>[41]</sup> g-C<sub>3</sub>N<sub>4</sub><sup>[42]</sup>

or graphene oxide<sup>[43]</sup> assisted the perovskite growth and led to improved photovoltaic efficiencies, in view of their high conductivity and high charge carrier density.

Here, the use of PbS NPLs improves the atomic interactions and in turn allows to achieve an organized perovskite growth. PbS NPL additives are beneficial to stimulate a favorable growth and orientation of FA<sub>0.9</sub>Cs<sub>0.1</sub>PbI<sub>3</sub> grains, to prevent degradation, and further to promote long-term stability of the material and of the solar cells, becoming a competitive strategy that exceeds the current stability standards at ambient temperature.<sup>[20,32]</sup> The low amount of structural defects is correlated to the improvement of the perovskite optoelectronic properties and of the solar cell reproducibility.<sup>[44]</sup> The increased stability is also demonstrated by the incident photon to current efficiency (IPCE) measurement, as the absorption of photons in the region 650–800 nm is preserved in the presence of PbS NPLs after 4 months, demonstrating the favorable effect of PbS NPLs not only on the stabilization of the formamidinium perovskite material, but above all on the solar cells with a more reproducible PCE of 19% for fresh-made devices and increased stability associated with the preservation of photon absorption in the infrared (IR) region of the electromagnetic spectrum, where frequently the light collection fails.<sup>[45,46]</sup> Interestingly this effect is observed for samples prepared both in glovebox with N<sub>2</sub> atmosphere or under ambient conditions in air with 50–55% relative humidity (RH).

## 2. Results and Discussions

PbS NPLs were synthesized according to the method reported by Khan et al.<sup>[38]</sup> Figure 1a,b shows the associated transmission electron microscopy (TEM) images. The average length is around 47.1 ± 6.5 nm. According to the photoluminescence (PL) features of NPLs (Figure 1c), their thicknesses are into the range of 1.8–2.3 nm.<sup>[38]</sup> Since the synthesized colloidal PbS NPLs have trioctylamine (TOA) and/or oleic acid (OA) as organic ligands, to make them compatible with perovskite matrix, it is necessary to replace these ligands by a FAPbI<sub>3</sub> shell; see ligand exchange details in Supporting Information and Figure S1, Supporting Information in which the energy dispersive X-ray spectroscopy (EDS) and the selected area electron diffraction (SAED) are reported to show the integrity of the PbS after the ligand exchange and the orthorhombic crystal structure. In order to confirm the formation of PbS NPLs before and after ligand treatment, high-resolution TEM (HR-TEM) measurements were performed (insets of Figure 1a,b). The (400) plane was also identified along the PbS NPLs, with an interplanar spacing of 0.27 nm. This plane is characteristic of the extended (100) facet of the orthorhombic phase.<sup>[38]</sup> After the ligand exchange, the PbS NPL length decreases to 38.2 ± 9.3 nm (Figure 1b). The steady state PL peak wavelength of the PbS NPLs lies at 740 nm, with a full width at half maximum (FWHM) around 57 nm, in accordance with a previous work.<sup>[38]</sup> For the PbS NPLs with perovskite precursors as ligands, we observed a blue-shift of 15 nm with a broader FWHM around 87 nm (Figure 1c). We can assume an increase of the size dispersion and a decrease of the average NPL width, caused by the extraction of the TOA/OA, as observed in the TEM image (Figure 1b). Thus the PbS QDs and NPLs have a different trend in the PL shift after

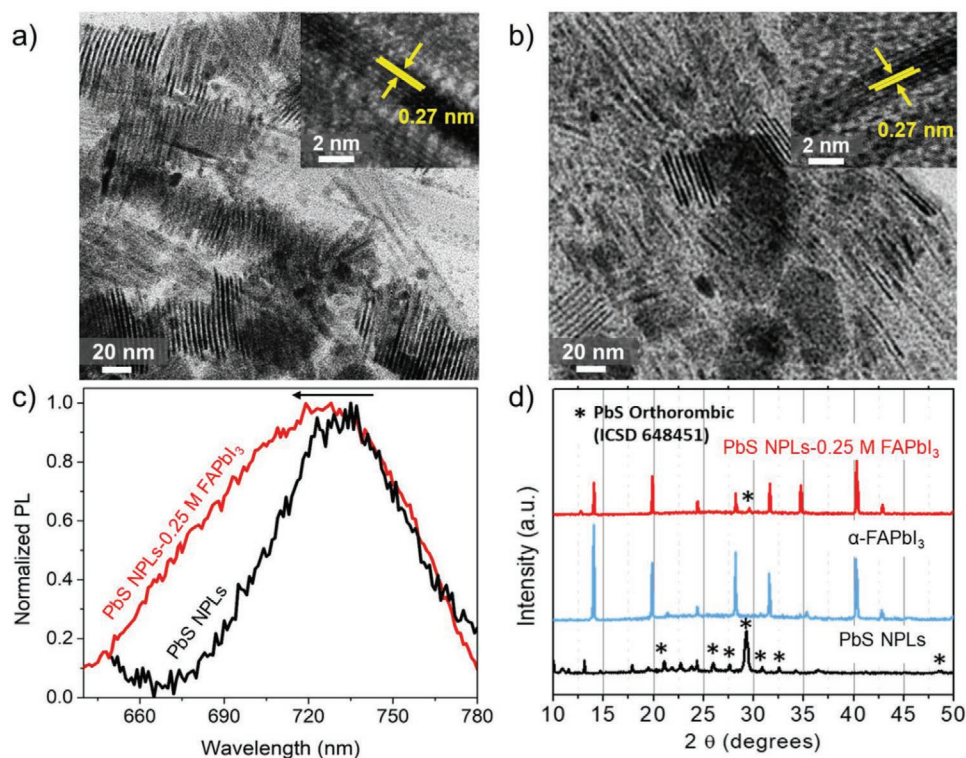


**Figure 1.** TEM images of PbS NPLs: a) Before ligand exchange; b) After ligand exchange. c) Steady state photoluminescence spectra of NPL samples, FWHM = 57 nm (black) before ligand exchange, and FWHM = 87 nm (red) afterward. d) XRD patterns of the PbS NPL samples before (black) and after (red) ligand exchange and of the FAPbI<sub>3</sub>  $\alpha$ -phase (blue); ICSD 250736; the asterisk shows the main peak of the PbS after the ligand exchange. HR-TEM images depicted as insets of Figure 1a,b show the characteristic (400) plane (extended [100] facet) of orthorhombic phase from PbS NPLs.

the ligand exchange, as for the former, the red-shift is due to the loss of the quantum confinement,<sup>[32]</sup> while for the latter, the reduced lateral dimensions result in a lateral confinement and in the blue-shift of the PL, common for the NPLs system with different ligand or shell.<sup>[47–50]</sup> This phenomenon is attributed to the shortened dimension of the exchanged ligand.<sup>[51]</sup> The X-ray diffraction (XRD) patterns show that the crystal structure is orthorhombic (ICSD 648451) before ligand exchange, see Figure 1d.<sup>[38]</sup> After ligand exchange, we observed peaks mainly associated with the  $\alpha$ -phase of the perovskite crystal structure. In this context, SAED patterns were obtained with the purpose to corroborate the crystalline phase of PbS NPLs without and with ligand exchange (Figure S1 b,b', Supporting Information). Thus, the diffraction planes were calculated by obtaining their interplanar spacings ( $d$ ). In both the materials,  $d$  values were estimated to be  $\approx 0.30$ , 0.27, and 0.21 nm, corresponding to (111) plane of the cubic phase (ICSD 38293), and (400) and (002) planes of the orthorhombic phase (ICSD 648451), respectively. These planes are associated to the extended (100) and (001) facets of this crystalline structure.<sup>[38]</sup> This result is in good agreement with the HR-TEM images. The cubic phase evidenced in the SAED patterns could be attributed to the emergence of some PbS nanoparticles formed together with the NPLs. However, according to the XRD pattern of the PbS NPLs shown in Figure 1d, the orthorhombic phase is the main crystalline structure in the materials as expected.

In order to prepare perovskite thin films with PbS NPL additives, the ratio between the perovskite FA<sub>0.9</sub>Cs<sub>0.1</sub>PbI<sub>3</sub> and

the PbS NPLs was varied upon a screening on the concentration of the NPLs.<sup>[32]</sup> A scanning electron microscopy (SEM) image of the pure FA<sub>0.9</sub>Cs<sub>0.1</sub>PbI<sub>3</sub> film shows a broad size distribution from 74 to 774 nm, with a majority of small grains, resulting in a mean size of 304 nm, Figure 2a and Table S1, Supporting Information. With the incorporation of PbS NPLs at 0.5 mg mL<sup>-1</sup>, see Figure 2b, the grains grow bigger, reaching a maximum size of 835 nm, with a mean of 330 nm (Table S1, Supporting Information). At higher concentration such as 1 and 1.5 mg mL<sup>-1</sup>, see Figures 2c,d, despite the presence of big grains (up to 870 nm), the smaller ones are predominant, resulting in a mean size of 275 and 281 nm, respectively (Table S1, Supporting Information). Thus, PbS NPLs have a role on the perovskite thin film growth process, but the concentrations need to be carefully optimized, to obtain a uniform distribution, see the statistical distribution in Figure S2 and Table S1, Supporting Information. It is worth noting that the cross-section images, see Figures 2e–h, clearly evidence a neat arrangement with a vertical orientation of the perovskite polycrystalline grains<sup>[28]</sup> in the sample with 0.5 and 1 mg mL<sup>-1</sup>, more oriented as compared to the 0 and 1.5 mg mL<sup>-1</sup> perovskite-PbS NPL layers, making sharp interfaces also on the top and on the bottom of the perovskite layer. Perovskite grains of samples at 0.5 mg mL<sup>-1</sup> extend mostly along all of the perovskite thickness, reducing the grain boundaries in the direction of carrier transport, perpendicular to the film.

To shed light on the effect that the PbS NPLs have on the crystallinity, XRD analysis was performed. The XRD spectra show the characteristics peaks of the FA<sub>0.9</sub>Cs<sub>0.1</sub>PbI<sub>3</sub>  $\alpha$ -phase



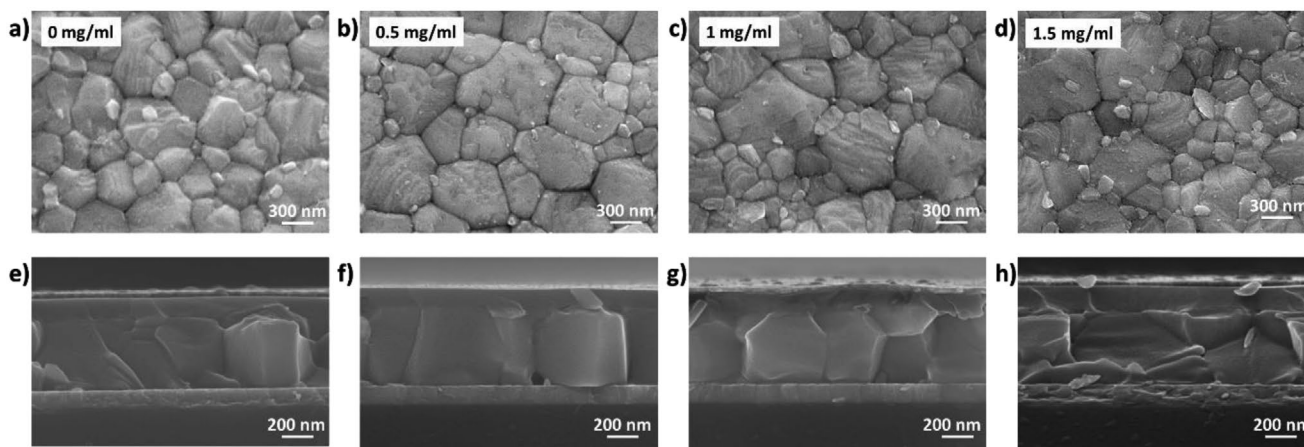


**Figure 2.** SEM top-view images of the films based on a)  $\text{FA}_{0.9}\text{Cs}_{0.1}\text{PbI}_3$ , b) with  $0.5 \text{ mg mL}^{-1}$  PbS NPLs, c) with  $1 \text{ mg mL}^{-1}$  PbS NPLs and d) with  $1.5 \text{ mg mL}^{-1}$  PbS NPLs. e–h) Corresponding SEM cross-section images.

(ICSD 250736) at  $14.03^\circ$  (100),  $20.08^\circ$  (110),  $24.32^\circ$  (111),  $28.20^\circ$  (200),  $31.62^\circ$  (120), and  $40.30^\circ$  (220),<sup>[32,52]</sup> see **Figure 3a**. The highest ratio between the (100) and (110) peak intensities is observed for the  $1 \text{ mg mL}^{-1}$  and especially for the  $0.5 \text{ mg mL}^{-1}$  samples, see Table S2, Supporting Information. It is indicative of the preferred growth over the (100) plane,<sup>[53]</sup> in line also with the SEM cross-sections images. It is worth noting that all samples with PbS NPLs are very stable, as the XRD patterns after

4 months in air (relative humidity of 20%) just show minor  $\text{PbI}_2$  peaks that, on the contrary, are more pronounced in the bare perovskite, see **Figure 3b**. Moreover we exposed the sample at  $55 \pm 15\%$  of relative humidity (RH) and the trend is confirmed (**Figure S3**, Supporting Information).<sup>[54]</sup> The improved halide perovskite stability, when PbS NPLs are embedded in the perovskite matrix, is strictly correlated to the bigger grain size and improved crystal orientation, less affected by the ambient

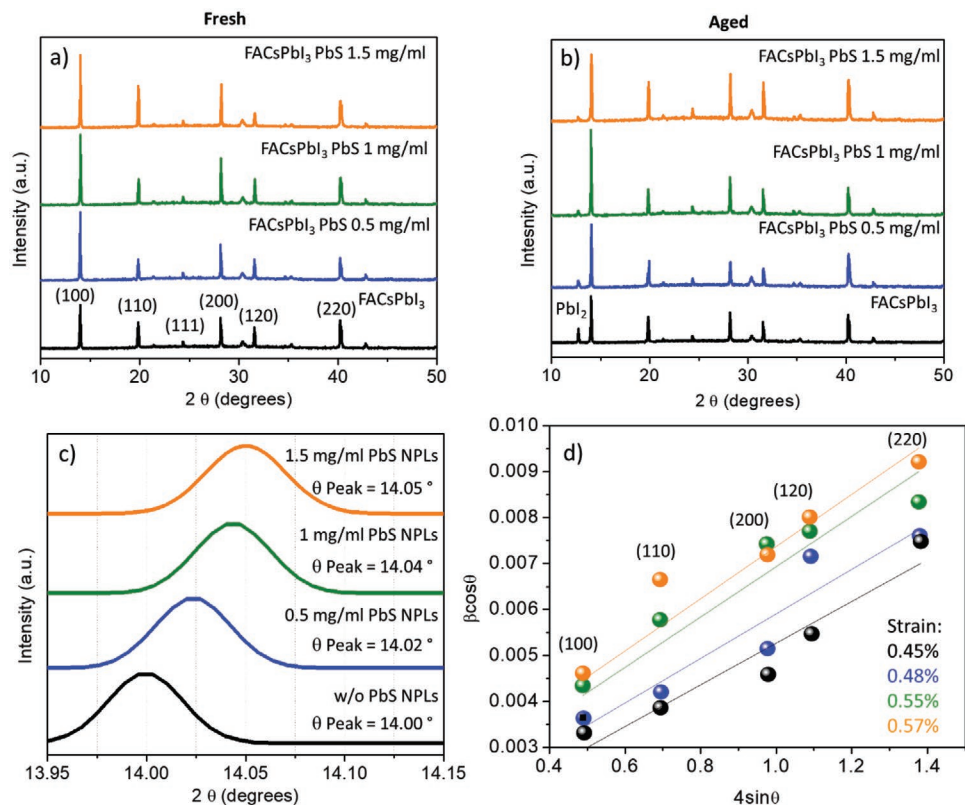


**Figure 3.** XRD diffraction patterns of the control sample and of the  $\text{FA}_{0.9}\text{Cs}_{0.1}\text{PbI}_3$  (ICSD 250736) on FTO substrates with different amounts of embedded PbS NPLs a) freshly made and b) aged for 4 months in air (relative humidity 20%). c) Gaussian fit of the magnified (100) peak of the perovskite XRD patterns with and without PbS NPLs; d) Williamson–Hall plot of the full width at half maximum (FWHM) corresponding to the XRD peaks. The strain is calculated as the slope of the linear fit.

conditions, but also to the lower surface energy reached after the interaction with the PbS NPLs. The latter effect is in fact the reason why at higher concentration of PbS NPLs, the perovskite is more stable than the perovskite without PbS NPLs, even if the grains were no more prevalently bigger and well ordered.<sup>[32]</sup> The interaction between the perovskite and the NPLs is quantified with Williamson–Hall analysis.<sup>[55]</sup> Upon increasing the NPL concentration, the peaks corresponding to the (100) and (200) planes shift (Figure 3c) and the strain is up to 26% higher than in the bare perovskite, see Figure 3d. The released strain is associated with the compression of the unit cell. As the FAPbI<sub>3</sub> perovskite has a tolerance factor close to 1, the unit cell compression determines a stabilization of the cells, associated to the improved interaction between the cation and the inorganic octahedra.<sup>[20]</sup> As the only difference between samples is the PbS NPL concentration, this increased strain can be attributed to the chemical interaction between the two materials, due to favorable matching between the NPL (100) crystal orientation and the perovskite  $\alpha$ -phase, where NPLs distort the perovskite lattice in a similar way as the substrate does on the layer that epitaxially grows on top of it.<sup>[32]</sup>

The optical properties of the four different samples, prepared with increasing PbS NPL concentration present similar light absorption spectra, see Figure 4a, with the absorption edge around 780 nm and a stable bandgap around  $\approx 1.55$  eV, see Figure 4b. Interestingly the PL emission spectra at open circuit conditions, Figure 4c, show an increase in the emission intensity for the 1 mg mL<sup>-1</sup> and especially for the 0.5 mg mL<sup>-1</sup> samples, pointing to a reduction of nonradiative recombination,<sup>[56]</sup> in line with the better grain arrangement observed in the SEM images, see Figure 2, and with the higher stability, see Figure 3. It is in fact well-known that the defects play a determining role in the degradation of the PSCs.<sup>[57]</sup>

The influence of PbS NPLs, observed beyond its effect on thin layers, is confirmed by the properties of the photovoltaic devices manufactured with them. The device architecture employed was ITO/SnO<sub>2</sub>/FA<sub>0.9</sub>Cs<sub>0.1</sub>PbI<sub>3</sub>-PbS NPLs/phenylethylammonium iodide/Spiro-OMeTAD/Au, see Figure S4a, Supporting Information. In Figure S4b and Table S3, Supporting Information, the figures of merit of the champion devices are reported. The devices are stable under operating conditions, and the obtained maximum photoconversion efficiency

(PCE) is, in all cases, close to 19% with negligible hysteresis, see Figure S5 and Table S3, Supporting Information, in line with previous reports.<sup>[23,58,59]</sup> The introduction of PbS NPLs at 0.5 and 1 mg mL<sup>-1</sup> does not interfere with the carrier extraction and collection, and a similar performance compared to the reference samples without NPLs is obtained, see Table S3, Supporting Information. For these samples, we measured a higher average open circuit potential,  $V_{oc}$ , than for the reference samples with no PbS NPLs, while a slightly lower fill factor, FF, was observed when NPLs were added, see Figure S5 and Table S3, Supporting Information. In fact, champion performance has been obtained for a sample with PbS NPLs (0.5 mg mL<sup>-1</sup>), where a stabilized efficiency was measured tracking the current density at maximum power point ( $J_{MPP}$ ), measured during 1000 s (Figure S4c,d, Supporting Information), assuring the system stability and its improvement. The reproducibility is also increased for samples with PbS NPLs at a concentration of 0.5 and 1 mg mL<sup>-1</sup>, see Figure S5b, Supporting Information. However, when a PbS NPLs concentration of 1.5 mg mL<sup>-1</sup> is used, a small but general reduction of all photovoltaic parameters is obtained, with the FF being the most affected, resulting in a clear reduction of the PCE and reproducibility, see Figure S5, Supporting information. This reduction of performance is a direct consequence of the inhomogeneous morphology of the active layer, see Figure 2d,h, which leads to the presence of more barriers and defects, triggering a poor charge transport in the matrix, in line with the reduced PL, see Figure 4c. The poor reproducibility of 1.5 mg mL<sup>-1</sup> is attributed to the agglomeration of PbS NPLs at this concentration in the film, triggering a nonuniform distribution of local strain, correlated with the inhomogeneous formation of defects and electronic traps.<sup>[60]</sup> Upon the agglomeration of the PbS NPLs, the interaction with the perovskite could be reduced as the NPLs expose only the lateral sides when agglomerated in stacks.<sup>[61]</sup>

These results highlight that the introduction of PbS NPLs with proper concentration does not decrease the photovoltaic device performance and even slightly improve reproducibility. In this sense, the impedance analysis, under the same illumination at different applied bias, see Figure S6a, Supporting Information, and at different light intensities, see Figure S6b, Supporting Information, unveiled that the recombination resistance<sup>[62]</sup> is slightly higher for samples with 0.5 mg mL<sup>-1</sup>

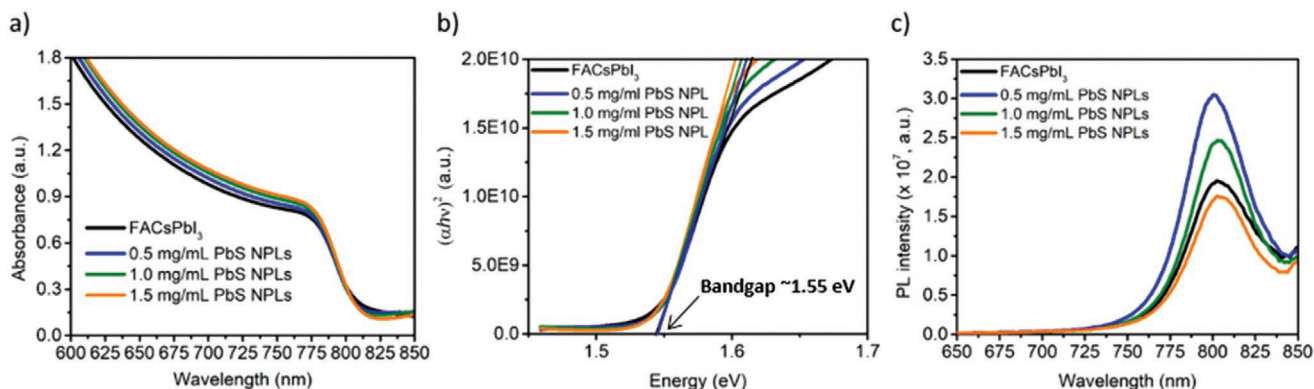


**Figure 4.** Optical properties of FA<sub>0.9</sub>Cs<sub>0.1</sub>PbI<sub>3</sub> films with different concentration of PbS NPLs: a) UV-vis absorbance spectra, b) Tauc plot (the bandgap is in all the cases  $\approx 1.55$  eV; the calculated bandgaps of the FACsPbI<sub>3</sub> with no NPLs, 0.5 mg mL<sup>-1</sup>, 1.0 mg L<sup>-1</sup> and 1.5 mg mL<sup>-1</sup> are 1.5465 eV, 1.568 eV, 1.5478 eV, and 1.5472 eV, respectively), and c) steady state PL of the perovskite-PbS NPL films on tin oxide (SnO<sub>2</sub>).

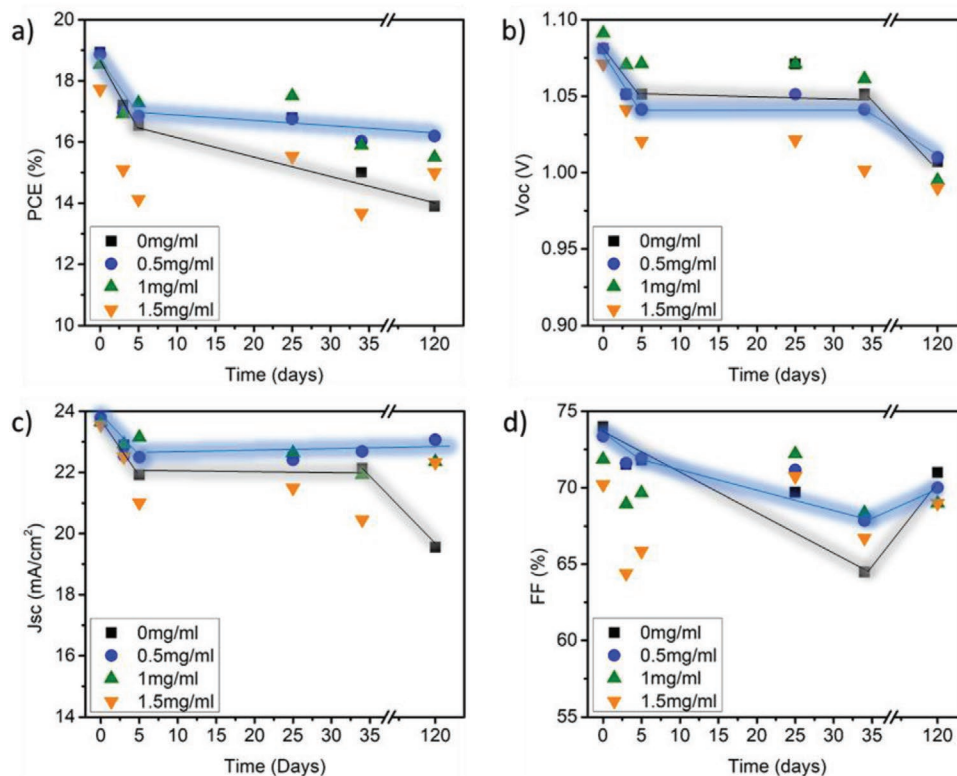


**Figure 5.** Evolution of the photovoltaic parameters of the solar cells from day 0 to day 120: a) power conversion efficiency, b) open circuit voltage, c) short circuit current, and d) fill factor. Samples were stored in dark conditions in air, at 25 °C and 35% of relative humidity.

PbS NPLs, confirming the reduction of nonradiative recombination as PL measurements already showed, see Figure 4c, and in good agreement with the higher  $V_{oc}$  when PbS NPLs with 0.5 mg mL<sup>-1</sup> concentration are used as additives, see Table S3, Supporting Information.

Beyond the slight increase on device performance and reproducibility after the addition of PbS NPLs, the most significant effect of the NPL incorporation is a significant enhancement of device stability under ambient conditions (25 °C and 35% of relative humidity). Figure 5 plots the evolution of the different photovoltaic parameters during 4 months. Further statistical analysis is described in Figure S7, Supporting Information. Figure 5 clearly highlights the stability improvement when PbS NPLs are incorporated, even with a concentration of 1.5 mg mL<sup>-1</sup>, showing that devices without PbS NPLs are less stable. Independently of the presence of PbS NPLs, all devices exhibit a reduction of the photovoltaic performance, from 19% to 15%, during the first 5 days, see Figure 5a, as a consequence of the reduction of  $J_{sc}$ . This burn-in effect has been observed repeatedly in n-i-p PSCs.<sup>[63]</sup> After the burn-in period,  $J_{sc}$  stabilizes for samples with NPLs while reference samples exhibit a continued decrease. Consequently, devices with 1 mg mL<sup>-1</sup> and especially 0.5 mg mL<sup>-1</sup> present the highest PCE stability in air, originating from a stable  $J_{sc}$  after burn-in period, for at least 4 months, see Figure 5, which compared with reported stability measurements in nitrogen, is a longer time and very promising for the concrete application of planar PSCs architecture.<sup>[12]</sup>

This finding demonstrates, once again, that the PbS-perovskite interaction leads to a stabilization of the material, attributable to the vertical orientation of the grains and improved

morphology due to the 2D NPL shape and to a preferential (100) surface structure, as deduced from the TEM of the PbS NPLs,<sup>[38]</sup> resulting in a highly efficient and stable device. The addition of the appropriate amount of PbS NPLs results in a longer stability of the devices, principally due to a reduction of the  $J_{sc}$  deterioration, as also pointed out by IPCE measurement of devices without and with 0.5 mg mL<sup>-1</sup> of PbS NPLs, see Figure 6. For fresh samples, Figure 6a, both have similar IPCE spectra between 300 and 810 nm and a maximum IPCE of 94% observed at 450 nm, while the sample with PbS NPLs shows a slightly higher performance at long wavelengths,  $\lambda > 725$  nm. Note that at 750 nm, a combined photogeneration from perovskite and PbS NPLs occurs, due to the similar bandgap, see Figures 1c and 4b. After 4 months, an impressive difference between the two spectra arises, see Figure 6b. The device without NPLs exhibits a small decrease of IPCE for  $\lambda < 450$  nm, and a more significant drop at longer wavelengths. The IPCE evolution is the sign of a partial degradation of the perovskite into species with higher bandgap, such as PbI<sub>2</sub>, see Figure S8, Supporting Information, responsible for a lower  $J_{sc}$  in aged devices, see Figure 5. In contrast, the aged sample with PbS NPLs presents just a small reduction of IPCE spectra compared to the fresh one, so the PbS NPL-perovskite interaction improves the stability but more important compensates for the commonly observed IPCE loss at longer wavelengths, from 600 to 820 nm in FA<sub>0.9</sub>CS<sub>0.1</sub>PbI<sub>3</sub>.<sup>[22,60]</sup> This improvement in the IPCE evidences indirectly a superior quality of the material, see Figure 3a, the sharp and well-optimized interfaces between the active and selective layers, see Figure 2f, and the stable injection of the electrons during the time. Moreover, we



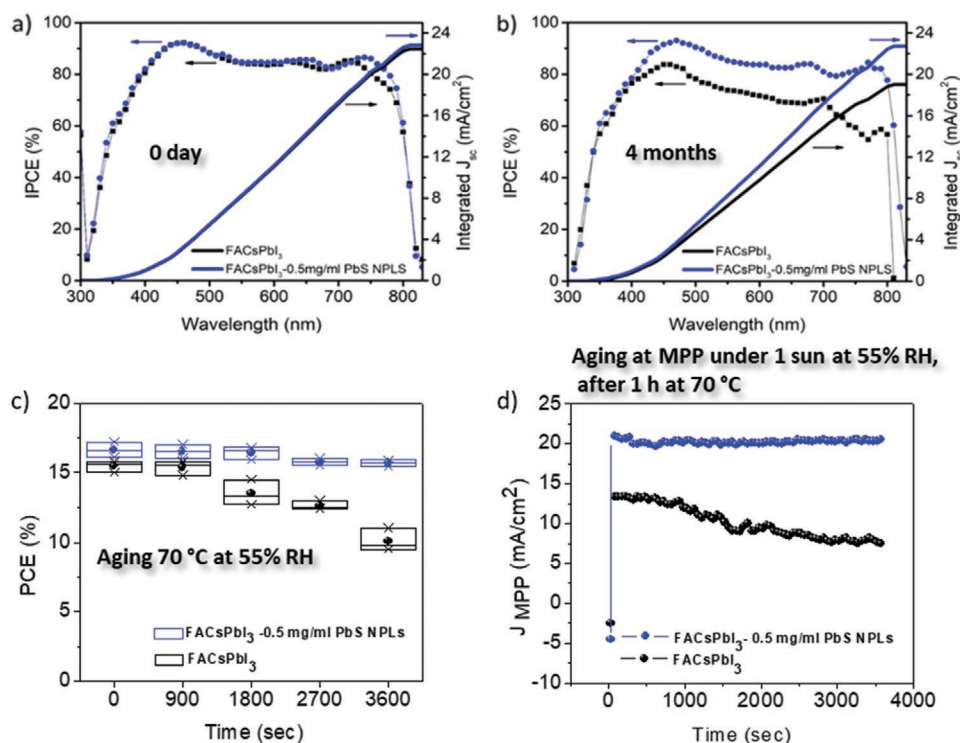


**Figure 6.** Incident photon to current efficiency curves and integrated photocurrent of 0 and 0.5 mg mL<sup>-1</sup> PbS NPLs-based devices at a) 0 day and b) after 4 months (25 °C and 35% of RH). c) Stability data of three devices with and without PbS NPLs after annealing under heating (70 °C, 55 ± 15% RH); d) Track of the current at maximum power point ( $V_{MPP}$  FACsPbI<sub>3</sub> = 0.786 V and  $V_{MPP}$  FACsPbI<sub>3</sub>-0.5 mg mL<sup>-1</sup> PbS NPLs = 0.853 V for 1 h under 1 sun illumination, after 1 h of heating at 70 °C in air, 55 ± 15% RH (see Figure 6c), of the devices with and without PbS NPLs. The device without NPLs degrades after 1 h at 70 °C in air, so the  $J_{MPP}$  is lower than the original value (see Figure S4c, Supporting Information). All the measurements were performed on devices without encapsulation.

performed photostability tests after heating and under higher humidity conditions (Figure 6c,d and Figure S9, Supporting Information). As is reported in Figure 6c, the devices without NPLs after an annealing in air (70 °C, 55 ± 15% RH, without encapsulation) start degrading after 30 min, while the devices with the NPLs are stable for 1 h of annealing. The most evident degradation of the control devices is after illumination at maximum power point (MPP) under 1 sun for 1 h (Figure 6d); here the current density decreases until reaching the 33% of its initial value. On the contrary the device with PbS NPLs is stable even after the illumination. This evidence is also valid without the pre-heating step (Figure S9, Supporting Information), indicating that the control device is almost stable after annealing, but under light, the degradation processes are superior than in the device with NPLs. Thus the PbS NPLs confer a huge stability either under moderate air conditions (ambient temperature and 35% RH), or under much stressed operational conditions such as higher humidity (55 ± 15%; 70 °C and under illumination at 1 sun). These results can be ascribed to the improved stability of the perovskite black phase and improved morphology, which assure reduced or suppressed ion migration under operational conditions, induced by light or the high temperatures.<sup>[54,64]</sup>

In order to corroborate the strong and robust impact of the PbS NPLs on device stability, the same devices were fabricated also under ambient conditions (in air, 25 °C and 50–55% RH). While the environmental surroundings usually play a dramatic role in achieving reproducible device performances and

properties,<sup>[65]</sup> the solar cell parameters of devices fabricated under ambient conditions, see Figure 7 and Figure S10, Supporting Information, show a similar trend as the ones fabricated under inert conditions,<sup>[66]</sup> and a record PCE of ≈17% is achieved with the addition of PbS NPLs with 0.5 mg mL<sup>-1</sup> concentration. It is worth to note that under these conditions the PbS NPLs have also more evident benefits, as the PCE of the device based on 0.5 mg mL of PbS NPLs is 7% higher than the control device, see Figure 7a, and is more reproducible, see Figure 7b.

### 3. Conclusions

In summary, FA<sub>0.9</sub>Cs<sub>0.1</sub>PbI<sub>3</sub> solar cells are successfully fabricated under nitrogen and ambient conditions (25 °C and 50–55% RH), obtaining a maximum PCE of 19% and 17%, respectively. In both cases, a higher performance has been obtained with the addition of PbS NPLs with 0.5 mg mL<sup>-1</sup> concentration into the perovskite matrix, with the improvement with respect to reference samples without NPLs, being more significant for devices fabricated under ambient conditions. We observed that PbS NPLs help to obtain a better crystallization of the perovskite film, with an ordered and uniform morphology due to the chemical interaction with the 2D PbS NPLs exhibiting a preferential (100) direction. Moreover, the solar cell characterization indicates that the devices without PbS NPLs show a reduction of photocurrent beyond the burn-in period, while upon the addition of 0.5 mg mL<sup>-1</sup> PbS NPLs, the stability of the

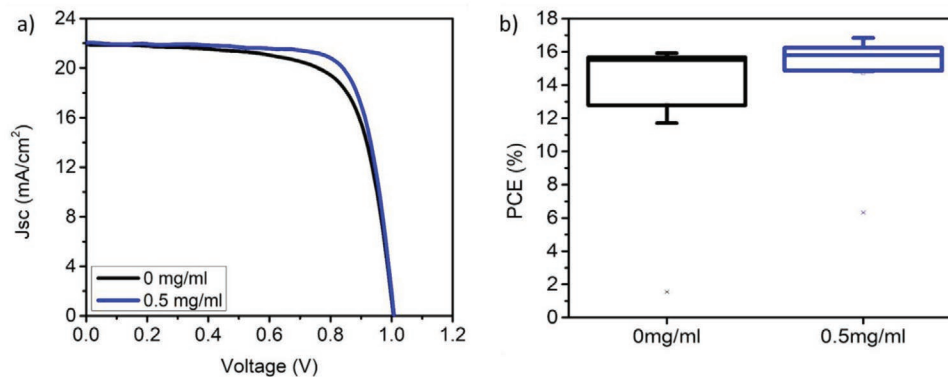


**Figure 7.** a)  $J$ - $V$  curves of the devices fabricated in air, at 25 °C and 50–55% RH, with  $\text{FA}_{0.9}\text{Cs}_{0.1}\text{PbI}_3$  without (black line) and with (blue line) 0.5  $\text{mg mL}^{-1}$  PbS NPLs as active layers. b) Statistical analysis of the PCE % on 20 solar cells, showing an improved reproducibility for devices with embedded PbS NPLs.

devices improved, maintaining  $J_{sc}$  above 23  $\text{mA cm}^{-2}$  for at least 4 months, a longer time than the stability measurements previously reported for planar solar cells, obtained also for unencapsulated samples stored at ambient conditions. In addition, the reproducibility of the devices fabricated under both inert and ambient atmosphere increases significantly by the addition of PbS NPLs with a concentration lower than 1.5  $\text{mg mL}^{-1}$ . Overall the PbS NPLs embedded in the  $\text{FA}_{0.9}\text{Cs}_{0.1}\text{PbI}_3$  material allow for a stable black phase perovskite film, simultaneously enabling stable, reproducible, and highly efficient photovoltaic devices.

## Supporting Information

Supporting Information is available from the Wiley Online Library or from the author.

## Acknowledgements

Financial support from the European Research Council (ERC) via Consolidator Grant (724424—No-LIMIT) and Starting Grant (714876 PHOCONA), EU (FEDER), MINECO under project TEC2017-85912-C2-2, Ministerio de Ciencia, Innovación y Universidades under project “Stable” PID2019-107314RB-I00, Generalitat Valenciana via Prometeo Grant Q-Devices (Prometeo/2018/098), and UJI project UJI-B2019-09 (DEPE2D) is gratefully acknowledged. H.E.S.-G. acknowledges CONACYT for the financial support for a short stay at INAM. E.A.E. also acknowledges support from Facultad de Ciencias Universidad de los Andes (Proyectos INV-2019-86-1798, INV2019-84-1828) and CEIBA foundation. Servei Central d'Instrumentació Científica (SCIC) from Universitat Jaume I is acknowledged for its help with SEM and XRD measurements and the SCSIE from the University of Valencia for providing TEM facilities.

## Conflict of Interest

The authors declare no conflict of interest.

## Author Contributions

S.M. and I.M.-S. conceived the project. A.F.G.-R., A.H.K., and I.M. synthesized the PbS NPLs and A.F.G.-R. performed the optical

characterization. H.E.S.-G. and E.A.E.-M. fabricated the solar cells and characterized them. S.M. performed the SEM and made the XRD analysis. S. A. and V. M.-S. conducted the TEM and EDS measurements of the materials. E.M.B. analyzed the impedance measurements. R.A.R., I.Z., P.O., and M.T.C. were involved in the student supervision and assisted in the work analysis. S.M. coordinated the experimental work. I.M.-S. coordinated the whole project. S.M., H.E.S.-G., and I.M.-S. wrote the manuscript. All the authors contributed to the discussions and revision of the manuscript.

## Keywords

formamidium, PbS nanoplatelets, perovskites, perovskite stability, reproducibility

Received: July 28, 2020  
Revised: September 28, 2020  
Published online:

- [1] P. V. Kamat, *ACS Energy Lett.* **2019**, *4*, 1055.
- [2] S. D. Stranks, G. E. Eperon, G. Grancini, C. Menelaou, M. J. P. Alcocer, T. Leijtens, L. M. Herz, A. Petrozza, H. J. Snaith, *Science* **2013**, *342*, 341.
- [3] N. Zhang, W. Sun, S. P. Rodrigues, K. Wang, Z. Gu, S. Wang, W. Cai, S. Xiao, Q. Song, *Adv. Mater.* **2017**, *29*, 1606205.
- [4] H. Dong, C. Zhang, X. Liu, J. Yao, Y. S. Zhao, *Chem. Soc. Rev.* **2020**, *49*, 951.
- [5] I. Suárez, E. J. Juárez-Pérez, J. Bisquert, I. Mora-Seró, J. P. Martínez-Pastor, *Adv. Mater.* **2015**, *27*, 6157.
- [6] Z.-K. Tan, R. S. Moghaddam, M. L. Lai, P. Docampo, R. Higler, F. Deschler, M. Price, A. Sadhanala, L. M. Pazos, D. Credgington, F. Hanusch, T. Bein, H. J. Snaith, R. H. Friend, *Nat. Nanotechnol.* **2014**, *9*, 687.
- [7] B. R. Sutherland, E. H. Sargent, *Nat. Photonics* **2016**, *10*, 295.
- [8] A. Fakharuddin, U. Shabbir, W. Qiu, T. Iqbal, M. Sultan, P. Heremans, L. Schmidt-Mende, *Adv. Mater.* **2019**, *31*, 1807095.
- [9] Best Research-Cell Efficiency Chart, <https://www.nrel.gov/pv/assets/pdfs/best-research-cell-efficiencies.20200925.pdf> (accessed: October 2020).
- [10] A. K. Jena, A. Kulkarni, T. Miyasaka, *Chem. Rev.* **2019**, *119*, 3036.
- [11] C. C. Stoumpos, C. D. Malliakas, M. G. Kanatzidis, *Inorg. Chem.* **2013**, *52*, 9019.
- [12] S.-H. Turren-Cruz, A. Hagfeldt, M. Saliba, *Science* **2018**, *362*, 449.



- [13] N. J. Jeon, J. H. Noh, Y. C. Kim, W. S. Yang, S. Ryu, S. I. Seok, *Nat. Mater.* **2014**, *13*, 897.
- [14] K. Wang, Z. Jin, L. Liang, H. Bian, D. Bai, H. Wang, J. Zhang, Q. Wang, S. Liu, *Nat. Commun.* **2018**, *9*, 4544.
- [15] C. J. Bartel, C. Sutton, B. R. Goldsmith, R. Ouyang, C. B. Musgrave, L. M. Ghiringhelli, M. Scheffler, *Sci. Adv.* **2019**, *5*, eaav0693.
- [16] W. Travis, E. N. K. Glover, H. Bronstein, D. O. Scanlon, R. G. Palgrave, *Chem. Sci.* **2016**, *7*, 4548.
- [17] E. J. Juarez-Perez, L. K. Ono, M. Maeda, Y. Jiang, Z. Hawash, Y. Qi, *J. Mater. Chem. A* **2018**, *6*, 9604.
- [18] T. M. Koh, K. Fu, Y. Fang, S. Chen, T. C. Sum, N. Mathews, S. G. Mhaisalkar, P. P. Boix, T. Baikie, *J. Phys. Chem. C* **2014**, *118*, 16458.
- [19] W. Shockley, H. J. Queisser, *J. Appl. Phys.* **1961**, *32*, 510.
- [20] S. Masi, A. F. Gualdrón-Reyes, I. Mora-Seró, *ACS Energy Lett.* **2020**, *5*, 1974.
- [21] J.-W. Lee, D.-J. Seol, A.-N. Cho, N.-G. Park, *Adv. Mater.* **2014**, *26*, 4991.
- [22] M. Hu, L. Liu, A. Mei, Y. Yang, T. Liu, H. Han, *J. Mater. Chem. A* **2014**, *2*, 17115.
- [23] J. W. Lee, D. H. Kim, H. S. Kim, S. W. Seo, S. M. Cho, N. G. Park, *Adv. Energy Mater.* **2015**, *5*, 1501310.
- [24] Y.-H. Lin, N. Sakai, P. Da, J. Wu, H. C. Sansom, A. J. Ramadan, S. Mahesh, J. Liu, R. D. J. Oliver, J. Lim, L. Aspitarte, K. Sharma, P. K. Madhu, A. B. Morales-Vilches, P. K. Nayak, S. Bai, F. Gao, C. R. M. Grovenor, M. B. Johnston, J. G. Labram, J. R. Durrant, J. M. Ball, B. Wenger, B. Stannowski, H. J. Snaith, *Science* **2020**, *369*, 96.
- [25] H. Zhang, M. K. Nazeeruddin, W. C. H. Choy, *Adv. Mater.* **2019**, *31*, 1805702.
- [26] S. Masi, A. Rizzo, R. Munir, A. Listorti, A. Giuri, C. Esposito Corcione, N. D. Treat, G. Gigli, A. Amassian, N. Stingelin, S. Colella, *Adv. Energy Mater.* **2017**, *7*, 1602600.
- [27] F. Xie, C.-C. Chen, Y. Wu, X. Li, M. Cai, X. Liu, X. Yang, L. Han, *Energy Environ. Sci.* **2017**, *10*, 1942.
- [28] X. Zheng, Y. Hou, C. Bao, J. Yin, F. Yuan, Z. Huang, K. Song, J. Liu, J. Troughton, N. Gasparini, C. Zhou, Y. Lin, D.-J. Xue, B. Chen, A. K. Johnston, N. Wei, M. N. Hedhili, M. Wei, A. Y. Alsalloum, P. Maity, B. Turedi, C. Yang, D. Baran, T. D. Anthopoulos, Y. Han, Z.-H. Lu, O. F. Mohammed, F. Gao, E. H. Sargent, O. M. Bakr, *Nat. Energy* **2020**, *5*, 131.
- [29] J. Xu, C. C. Boyd, Z. J. Yu, A. F. Palmstrom, D. J. Witter, B. W. Larson, R. M. France, J. Werner, S. P. Harvey, E. J. Wolf, W. Weigand, S. Manzoor, M. F. A. M. van Hest, J. J. Berry, J. M. Luther, Z. C. Holman, M. D. McGehee, *Science* **2020**, *367*, 1097.
- [30] Y. Zhang, S. Seo, S. Y. Lim, Y. Kim, S.-G. Kim, D.-K. Lee, S.-H. Lee, H. Shin, H. Cheong, N.-G. Park, *ACS Energy Lett.* **2020**, *5*, 360.
- [31] H. Min, M. Kim, S.-U. Lee, H. Kim, G. Kim, K. Choi, J. H. Lee, S. I. Seok, *Science* **2019**, *366*, 749.
- [32] S. Masi, C. Echeverría-Arrondo, K. M. M. Salim, T. T. Ngo, P. F. Mendez, E. López-Fraguas, D. F. Macias-Pinilla, J. Planelles, J. I. Climente, I. Mora-Seró, *ACS Energy Lett.* **2020**, *5*, 418.
- [33] S.-S. Li, C.-H. Chang, Y.-C. Wang, C.-W. Lin, D.-Y. Wang, J.-C. Lin, C.-C. Chen, H.-S. Sheu, H.-C. Chia, W.-R. Wu, *Energy Environ. Sci.* **2016**, *9*, 1282.
- [34] J. Han, S. Luo, X. Yin, Y. Zhou, H. Nan, J. Li, X. Li, D. Oron, H. Shen, H. Lin, *Small* **2018**, *14*, 1801016.
- [35] T. T. Ngo, S. Masi, P. F. Mendez, M. Kazes, D. Oron, I. M. Seró, *Nanoscale Adv.* **2019**, *1*, 4109.
- [36] B. Sun, A. Johnston, C. Xu, M. Wei, Z. Huang, Z. Jiang, H. Zhou, Y. Gao, Y. Dong, O. Ouellette, X. Zheng, J. Liu, M.-J. Choi, Y. Gao, S.-W. Baek, F. Laquai, O. M. Bakr, D. Ban, O. Voznyy, F. P. García de Arquer, E. H. Sargent, *Joule* **2020**, *4*, 1542.
- [37] Q. A. Akkerman, B. Martín-García, J. Buha, G. Almeida, S. Toso, S. Marras, F. Bonaccorso, U. Petralanda, I. Infante, L. Manna, *Chem. Mater.* **2019**, *31*, 8145.
- [38] A. H. Khan, R. Brescia, A. Polovitsyn, I. Angeloni, B. Martín-García, I. Moreels, *Chem. Mater.* **2017**, *29*, 2883.
- [39] H. Li, D. Zhitomirsky, J. C. Grossman, *Chem. Mater.* **2016**, *28*, 1888.
- [40] Y. Bi, A. Bertran, S. Gupta, I. Ramiro, S. Pradhan, S. Christodoulou, S.-N. Majji, M. Z. Akgul, G. Konstantatos, *Nanoscale* **2019**, *11*, 838.
- [41] V. Kamysbayev, A. S. Filatov, H. Hu, X. Rui, F. Lagunas, D. Wang, R. F. Klie, D. V. Talapin, *Science* **2020**, *369*, 979.
- [42] L.-L. Jiang, Z.-K. Wang, M. Li, C.-C. Zhang, Q.-Q. Ye, K.-H. Hu, D.-Z. Lu, P.-F. Fang, L.-S. Liao, *Adv. Funct. Mater.* **2018**, *28*, 1705875.
- [43] J.-S. Yeo, R. Kang, S. Lee, Y.-J. Jeon, N. Myoung, C.-L. Lee, D.-Y. Kim, J.-M. Yun, Y.-H. Seo, S.-S. Kim, S.-I. Na, *Nano Energy* **2015**, *12*, 96.
- [44] F. Wang, S. Bai, W. Tress, A. Hagfeldt, F. Gao, *NPJ Flexible Electron.* **2018**, *2*, 22.
- [45] M. Hao, Y. Bai, S. Zeiske, L. Ren, J. Liu, Y. Yuan, N. Zarrabi, N. Cheng, M. Ghasemi, P. Chen, M. Lyu, D. He, J.-H. Yun, Y. Du, Y. Wang, S. Ding, A. Armin, P. Meredith, G. Liu, H.-M. Cheng, L. Wang, *Nat. Energy* **2020**, *5*, 79.
- [46] H. Li, C. Chen, J. Jin, W. Bi, B. Zhang, X. Chen, L. Xu, D. Liu, Q. Dai, H. Song, *Nano Energy* **2018**, *50*, 699.
- [47] M. Li, M. Zhi, H. Zhu, W.-Y. Wu, Q.-H. Xu, M. H. Jhon, Y. Chan, *Nat. Commun.* **2015**, *6*, 8513.
- [48] J. Cherusseri, S. J. Varma, B. Pradhan, J. Li, J. Kumar, E. Barrios, M. Z. Amin, A. Towers, A. Gesquiere, J. Thomas, *Nanoscale* **2020**, *12*, 10072.
- [49] H. Huang, L. Polavarapu, J. A. Sichert, A. S. Susha, A. S. Urban, A. L. Rogach, *NPG Asia Mater.* **2016**, *8*, e328.
- [50] J. Shamsi, Z. Dang, P. Bianchini, C. Canale, F. Di Stasio, R. Brescia, M. Prato, L. Manna, *J. Am. Chem. Soc.* **2016**, *138*, 7240.
- [51] Y. Jiang, W.-S. Ojo, B. Mahler, X. Xu, B. Abécassis, B. Dubertret, *ACS Omega* **2018**, *3*, 6199.
- [52] M. Fu, P. Tamarat, J.-B. Trebbia, M. I. Bodnarchuk, M. V. Kovalenko, J. Even, B. Lounis, *Nat. Commun.* **2018**, *9*, 3318.
- [53] G. Zheng, C. Zhu, J. Ma, X. Zhang, G. Tang, R. Li, Y. Chen, L. Li, J. Hu, J. Hong, Q. Chen, X. Gao, H. Zhou, *Nat. Commun.* **2018**, *9*, 2793.
- [54] S. Akin, E. Akman, S. Sonmezoglu, *Adv. Funct. Mater.* **2020**, *30*, 2002964.
- [55] D. Nath, F. Singh, R. Das, *Mater. Chem. Phys.* **2020**, *239*, 122021.
- [56] M. Stolterfoht, V. M. Le Corre, M. Feuerstein, P. Caprioglio, L. J. A. Koster, D. Neher, *ACS Energy Lett.* **2019**, *4*, 2887.
- [57] S. P. Dunfield, L. Bliss, F. Zhang, J. M. Luther, K. Zhu, M. F. A. M. van Hest, M. O. Reese, J. J. Berry, *Adv. Energy Mater.* **2020**, *10*, 1904054.
- [58] A. Mahapatra, D. Prochowicz, M. M. Tavakoli, S. Trivedi, P. Kumar, P. Yadav, *J. Mater. Chem. A* **2020**, *8*, 27.
- [59] J. Troughton, N. Gasparini, D. Baran, *J. Mater. Chem. A* **2018**, *6*, 21913.
- [60] T. Hwang, A. J. Yun, J. Kim, D. Cho, S. Kim, S. Hong, B. Park, *ACS Appl. Mater. Interfaces* **2019**, *11*, 6907.
- [61] R. Young, *Structural Integrity and Durability of Advanced Composites*, Elsevier, Manchester, UK **2015**.
- [62] S.-M. Yoo, S. J. Yoon, J. A. Anta, H. J. Lee, P. P. Boix, I. Mora-Seró, *Joule* **2019**, *3*, 2535.
- [63] M. Saliba, M. Stolterfoht, C. M. Wolff, D. Neher, A. Abate, *Joule* **2018**, *2*, 1019.
- [64] N. Li, Y. Luo, Z. Chen, X. Niu, X. Zhang, J. Lu, R. Kumar, J. Jiang, H. Liu, X. Guo, B. Lai, G. Brocks, Q. Chen, S. Tao, D. P. Fenning, H. Zhou, *Joule* **2020**, *4*, 1743.
- [65] L. Contreras-Bernal, A. Riquelme, J. J. Gallardo, J. Navas, J. Idígoras, J. A. Anta, *ACS Sustainable Chem. Eng.* **2020**, *8*, 7132.
- [66] P. F. Méndez, S. K. M. Muhammed, E. M. Barea, S. Masi, I. Mora-Seró, *Sol. RRL* **2019**, *3*, 1900191.